FIZIKA 9 (1977) Supplement 3, 315–344
(Proceedings of the Int. Symp. on Nuclear Collisions and
Their Microscopic Description, Bled, September 1977)

Heavy Ion Scattering in 3D TDHF

M. S. Weiss
Lawrence Livermore Laboratory, University of California
Livermore, California 94550 U.S.A.

The material I will present are the results of calculations of three dimensional (3D) Time Dependent Hartree-Fock (TDHF) and breaks into three sections. The first, in collaboration with Hubert Flocard and Steve Koonin, are a series of results for $O^{16} + O^{16}$, primarily at E_{lab} = 105 MeV, but with other energies from 16 MeV to 200 MeV laboratory energy also studied.

To briefly remind you of the origins of TDHF, in Fig. 1, the action J is varied with respect to $\psi_i^*(r,t)$, which yields the equation for $\psi_j(r,t)$, with h(t) as described. The potential we have employed differs from that used in the calculations Dr. Maruhn has discussed in the previous talk primarily by the inclusion of the Yukawa term $W_y(r)$. This term, which is required for the surface properties, is extremely important and as I will indicate later leads to qualitatively different results from that used in Dr. Maruhn's calculation. This work also differs from that of the previous speaker in that we have always started by "pushing" self-consistent solutions of the static Hartree-Fock equations in 3D calculated with the same potential with which the dynamic equations were evolved. This insures that any nuclear excitation originates in the collision process. We start our solutions with 16 fm separation between their centers of mass and use a 1 fm mesh.

We impose spin and iso-spin independence; hence, each orbit is occupied by four nucleons. In addition we require reflection symmetry

in the reaction plane and point symmetry with respect to the center of mass. This permits us to actually solve the equations only in the volume outlined in Fig. 2. However, it also limits us to symmetric systems. This will be relaxed in the last part of this talk.

I will not discuss the techniques in any detail as they will shortly be available as a publication.[1] However, to succinctly delineate our procedure from that used in the previous talk, we work entirely in coordinate space, propagate the equations by expanding the exact Hamiltonian in an operator power series. Adjusting the time step and the number of terms in the series enables us to conserve energy to better than 1 MeV over the entire propagation time and the norm to 1 part in 10^{-5}. For the results presented here we have expanded to the fourth power of π and used a time step of $4 \cdot 10^{-24}$ sec. This conservatively fulfills our requirements.

Let us discuss $O^{16} + O^{16}$ at E_{lab} = 105 MeV as a function of impact parameter. In Fig. 3 is shown the iso-density contours integrated perpendicular to the reaction plane for $l = 5.5\hbar$ as a function of time, which is in units of 10^{-22} sec. This corresponds to a deeply inelastic collision and nearly backward scattering. In Fig. 4 we show the integrated iso-density contour as a function of time for an impact parameter corresponding to $l = 13\hbar$. We choose to call this system fused. (We have no sharp definition for fusion in this theory. But if the system stays together for so long that one could expect that a significant amount of de-excitation occurs through processes other than those in this model, then it is reasonable to expect that it has fused. Alternatively if the system rotates through such a grossly large angle that the graph of scattering angle vs impact parameter would have no pretense at continuity, then it is also reasonable to assume the system has fused; other equally subjective definitions are possible.) Figure 5 shows the same system

for $l = 39.5\ \hbar$, which is a Coulomb trajectory with negligible nuclear interaction.

At this energy, for $O^{16} + O^{16}$, we have examined many impact parameters; and in Fig. 6 we have the trajectories of the relative distance between the centers of mass of the two nuclei as a function of impact parameter. One sees that at small l the system bounces backwards, the scattering angle moves downward from the nearly Π at $l = 0.5\ \hbar$ to nearly $\Pi/2$ at $\ell = 10.5\ \hbar$ and then at $l = 13\ \hbar$ fusion begins. After $l = 27\ \hbar$ this ends and we have inelastic scattering until the impact parameter exceed the range of the nucleus interaction at $l = 40\ \hbar$. One notes that for small impact parameter there is a minimum radius beyond which the nuclei do not penetrate. This leads, naturally, to the concept of a repulsive potential and construction of an effective well with dissipation is dicussed in Ref. 1. It is instructive to examine some of the trajectories for those impact parameters that fuse. In Fig. 7 one can see the finely structured nature of these. At the little node points the system essentially comes to rest, the external angular momentum has been transferred to internal degrees of freedom, and in fact the system rotates backward for a moment. We believe this is due to the interaction of the single particle degrees of freedom with the collective angular momentum. The single particle wave functions spill into the newly formed collective well and in the process of reflecting from the far wall of the second nucleus cause these anomalies. It would clearly be difficult for a theory employing only collective variables to develop a large negative moment of inertia. If one needed to describe orbits such as these, the microscopic degrees of freedom must be explicitly included.

In the next figure (Fig. 8) the single particle energies for the $l = 2.5\ \hbar$ collision are shown. The definition single particle energy is arbitrary. These are the expectation values of the single particle

Hamiltonian. One notes that the initial degeneracy of the separated nuclei is broken when the wells overlap. They do not return to their original values when the nuclei separates due to internal excitation.

There is no clear interpretation of the physical content of this theory. Even if information enabling statements relating to individual channels is contained in this theory, no one has as yet extracted it. It is possible that TDHF represents the propagation of a quantity that has already been averaged over channels. In any case when comparing to experiments, we will assume that our results indicate a dominate process. With this ad hoc prescription in mind, we summarize in Fig. 9 our results for this energy. At the top the scattering angle vs impact parameter. At the bottom the energy loss vs impact parameter. The shaded area represents fusion where these quantities are not defined. The region of deep inelastic scattering has two sources: the region of small initial angular momentum before the onset of fusion, and another smaller region at larger impact parameter just exceeding that at which fusion ends. The latter was expected, the former was not. A consequence is a prediction of the theory that there will be highly-excited, slowly-moving fragments at very small angles going forward in the laboratory, which should provide an experimental test.

We found the phenomena of deeply inelastic scattering without fusion for small impact parameters quite interesting. An impact parameter of 6 fm seems maximum, at least at E_{lab} = 105 MeV. As you can see from Fig. 10, it is too large for E_{lab} = 32 MeV and the nuclei scatter. If we double the energy to E_{lab} = 64 MeV, maintaining the impact parameter b = 6 fm, you can see in Fig. 11 that we have fusion. If the density plot does not convince you, in Fig 12 we show the distance of the center

of mass of one nucleus from the center of mass of the system. Clearly, the nuclei are settling in as this radius slowly decreases with each vibration.

In Fig. 13 we have displayed the density for E_{lab} = 192 MeV, ℓ = 42 $\hbar$ in order to attempt to delineate the fusion region in both energy and impact parameter space. Due to the high energy, the complicated vibrations of the fused system are more dramatic than at lower energy. Note how the shape appears to become more compact with time.

The last figure in this part, Fig. 14, shows a summary of our knowledge of the fusion region for $O^{16} + O^{16}$ as a function of energy. The ⊕ represent fusion, the + scattering, the dotted curve our speculation for the shape of the fusion region which would be any point interior to the dotted curve. The listener may supply for himself the appropriate uncertainties in this curve but clearly the non-fusion region for "small" impact parameters is an increasingly important effect as the energy increases.

Heavy ion experiments have frequently relied upon the "reasonable" interpretation that fusion occurs at small impact parameter, followed by a region of impact paramters that lead to deeply inelastic scattering, etc. In this theory we see that for $O^{16} + O^{16}$ it is true for only a small region in energy, and that it becomes increasingly bad as the energy increases. Also, in this theory most of the deeply inelastic scattering comes from <u>small</u> impact parameters and the process of fitting critical angular momentum, etc., could be completely incorrect.

Now that we have disposed of the $o^{16} + o^{16}$ system, in this next part I will discuss our results for $Ca^{40} + Ca^{40}$ at E_{lab} = 278 MeV. This work and the next part were done in collaboration with H. Flocard, and

this system and energy were choosen so that we could compare with the extensive 2D calculations of Koonin *et al.*[2] In Ref. 2 the 2D TDHF equations are solved in a rotating coordinate system augmented by a prescription for the moment of inertia when the fragments are not separated. Let us first pay respect to art in Fig. 15-17 which shows the now familiar density profiles for $Ca^{40} + Ca^{40}$, $E_{lab} = 278$ MeV, $l = 20\ \hbar$, $70\ \hbar$, and $75\ \hbar$, respectively. You will note how inelastic scattering gives way to fusion and then again to inelastic scattering. The first point to note is the fact that our system fused at this energy, whereas in 2D it did not. Being somewhat more time consuming, we have not explored many impact parameters. In Fig. 18 we show the trajectories for those we have calculated. Again, small impact parameters lead to scattering, $l = 30\ \hbar$ fuses (the nuclei are together for more than $30 \cdot 10^{-22}$ sec), as does $l = 70\ \hbar$ (fusion exceeds $40 \cdot 10^{-22}$ sec and the "scattering angle" is in excess of $-3\ \pi$).

A more quantitative comparison with the results of Ref. 2 can be seen in the next figure (Fig. 19). Here we have plotted the energy loss vs incident angular momentum from Ref. 2 as the continuous line and imposed our results as ⊕. We basically find agreement before the onset of fusion (the shaded region in the figure) but much more energy loss in 3D after fusion. In Fig. 20 we made a similar comparison for the scattering angle. Where the 3D does not fuse, the agreement is excellent for small impact parameters, less so for larger. From this we conclude that there are no great instabilities in 3D vs 2D at small impact parameters and perhaps in regimes which do not fuse 2D may be an adequate theory or at lower energy.

We are in the process of examining the $Ca^{40} + Ca^{40}$ system for higher

energies and have nearly completed this for E_{lab} = 560 MeV. Bonche and Grammaticos[3] have examined the fusion cross section for Ca^{40} + Ca^{40} for 100 MeV < E_{lab} < 200 MeV. Combining these results we do not find any new phenomena and qualitatively the results for Ca^{40} are completely consistent with our experience for O^{16}. The charge distribution of the final fragments calculated in Ref. 2 were considerably too small relative to experiment. While the information to secure this from the results of our 3D calculations has been stored, the calculations have not yet been performed. Whether these will be wider than those of the 2D calculations and in better agreement with experiment because of the extra degrees of freedom remains to be seen.

In the last part of this talk I would like to show five viewgraphs for asymmetric systems. Here the point symmetry through the center of mass of the total system has been broken. These results were obtained shortly before I left for Slovenia and have not yet been completely analyzed. However, they are somewhat intriguing, if only as computer art. In Fig. 21 we have the now familiar density profiles for He^4 on O^{16} at $\ell = 5\hbar$, E_{lab} = 50 MeV. As you can see the apparent fusion is illusory and a light fragment, with at least approximately the average number of nucleons as the projectile, comes through. With our symmetries He^4 corresponds to one orbit, and it is serendipitous to think this is meaningful for a self-consistent mean field.

The next set, O^{16} on Ca^{40} at E_{lab} = 315 MeV, is intended to be significant as this corresponds to an experimentally observable situation. Figure 22 shows $\ell = 20\hbar$, the light fragment comes through; Fig. 23 ℓ = $40\hbar$, the light fragment comes through and appears to be diffracted; Fig. 24 $\ell = 60\hbar$, apparent fusion; and in Fig. 25 $\ell = 80\hbar$, a peripheral

collision. To the extent that we can tell from this very preliminary work, the light fragment maintains the same average number of nucleous as it started with. Whether this is a consequence of the relatively high energy, the several symmetries which inhibit transfer, or is a property of the TDHF theory remains to be seen. In addition we leave open the question of nuclear emission, which we have not seen.

In summary, I have attempted to show you some of the consequences of TDHF. While it is a theory with many uncertainties in its interpretation, it clearly is capable of making statements relative to reality. The validity of those statements must await experiment.

This work was performed under the auspices of the U. S. Energy Research and Development Administration under contract No. W-7405-Eng-48.

References

1. H. Flocard, S. E. Koonin, and M. S. Weiss, to be published.
2. S. E. Koonin et al., *Phys. Rev. C* 15, 1359 (1977).
3. P. Bonche and B. Grammaticos, contribution to the International Conference on Nuclear Structure, Tokyo, 1977.

$$J = \int_{t_1}^{t_2} dt \; \langle \Psi(t) \mid i\hbar \frac{\partial}{\partial t} - H \mid \Psi(t) \rangle$$

$$i\hbar \frac{\partial \psi_j}{\partial t} = h(t)\,\psi_j \qquad\qquad j = 1, \quad \text{—A.}$$

$$h = \frac{\hbar^2}{\partial m}\,\Delta^2 + \frac{3}{4}t_0\,\rho + \frac{3}{16}t_3\,\rho^2 + w_y + w_c$$

$$w_y(\vec{r}) = v_0 \int d\vec{r}' \frac{e^{-|\vec{r}-\vec{r}'|/a}}{|\vec{r}-\vec{r}'|/a}\;\rho(\vec{r}')$$

$$w_c(\vec{r}) = e^2 \int d\vec{r}' \frac{1}{|\vec{r}-\vec{r}'|}\;\rho_p(\vec{r}')$$

Fig. 1: The basic equations of TDHF theory and the specific Hamiltonian used in this work.

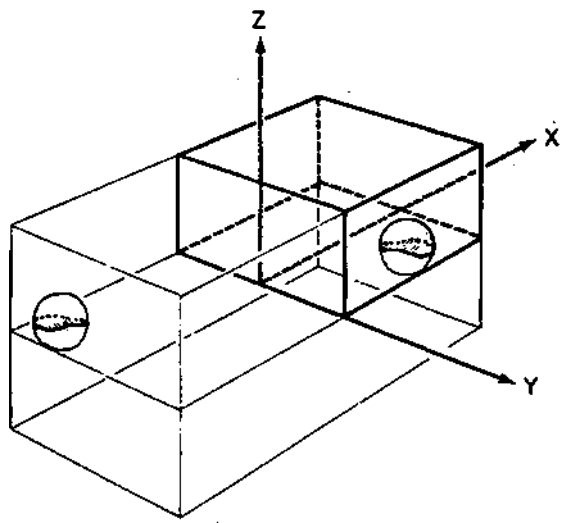

XBL 777-1528

Fig. 2: The volume inside the heavy black lines is the region of coordinate space that must be used for symmetric collisions.

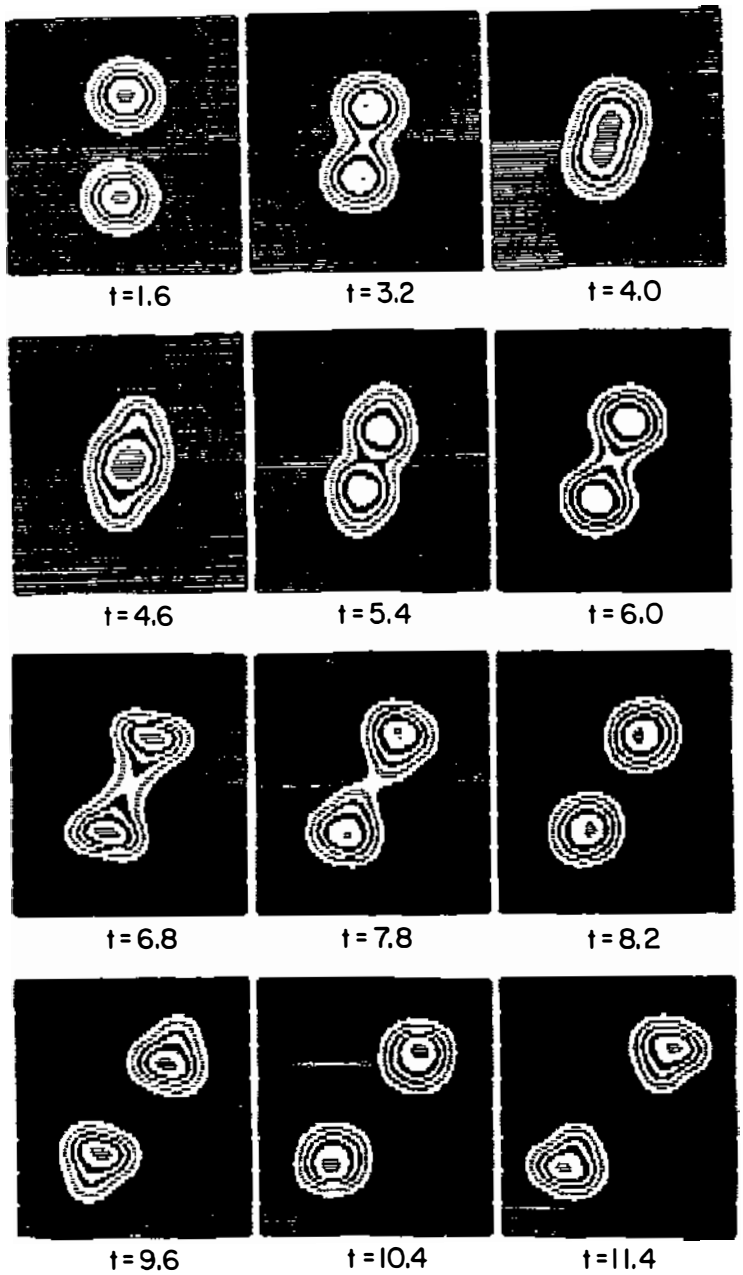

Fig. 3: Contour lines of the density integrated over the direction normal to the scattering plane. The collision corresponds to $O^{16} + O^{16}$ at E_{lab} = 105 MeV, incident angular momentum 5.5 $\hbar$, the times are in units of 10^{-22} sec.

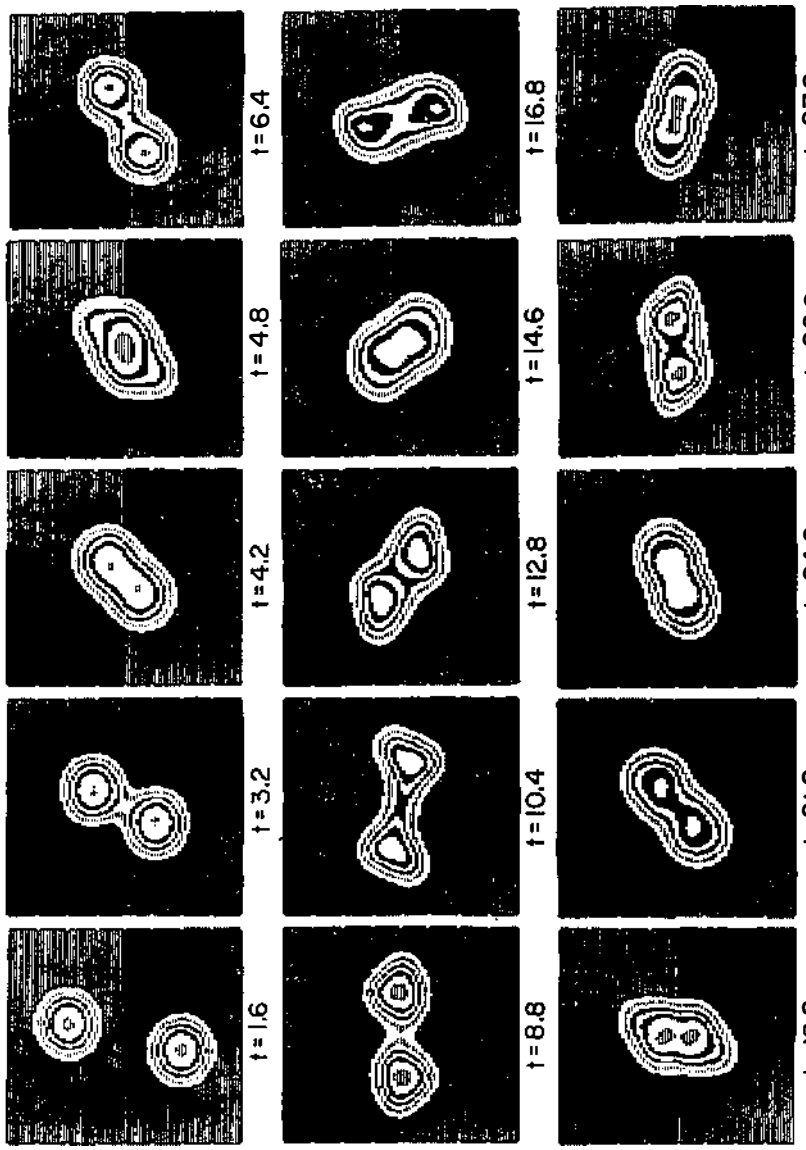

Fig. 4: Similar to Fig. 3 for incident angular momentum 13 ħ.

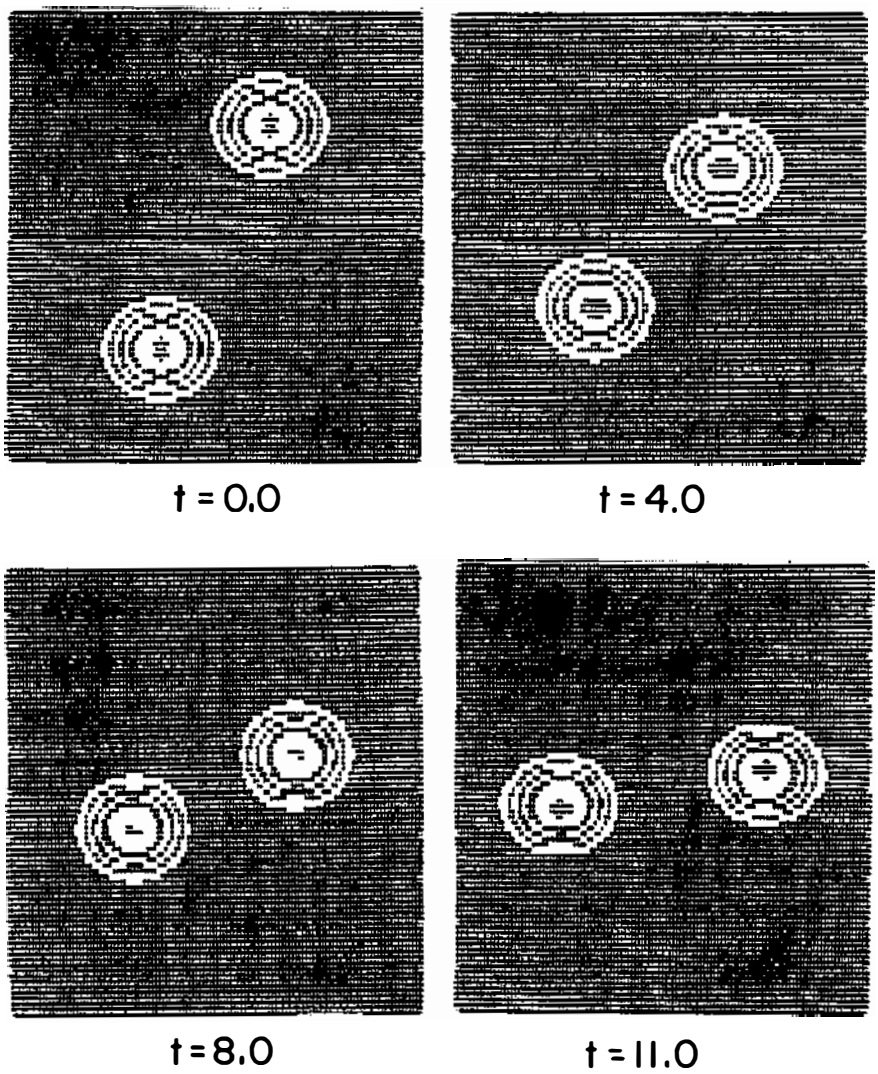

Fig. 5: Similar to Fig. 3 for incident angular momentum 39.5 $\hbar$. The time interval between the sections is 2.10^{-22} sec.

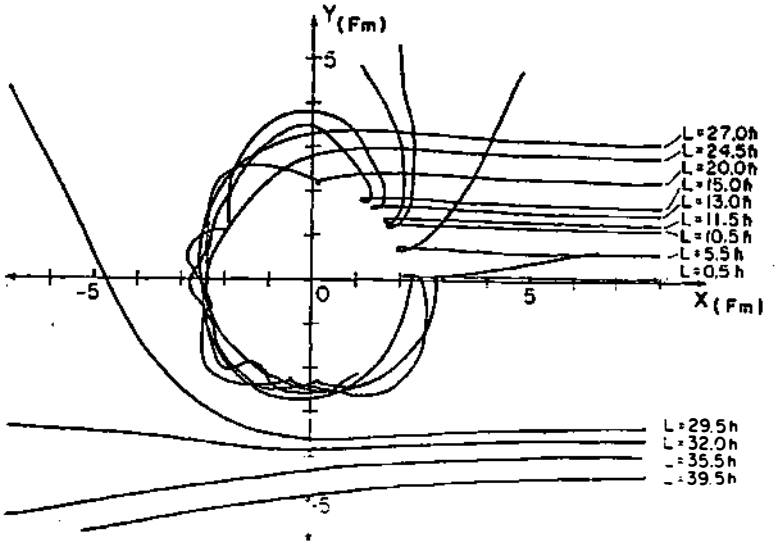

Fig. 6: The path of the vector between the centers of mass of the two nuclei, at E_{lab} = 105 MeV, for a variety of incident angular momentum.

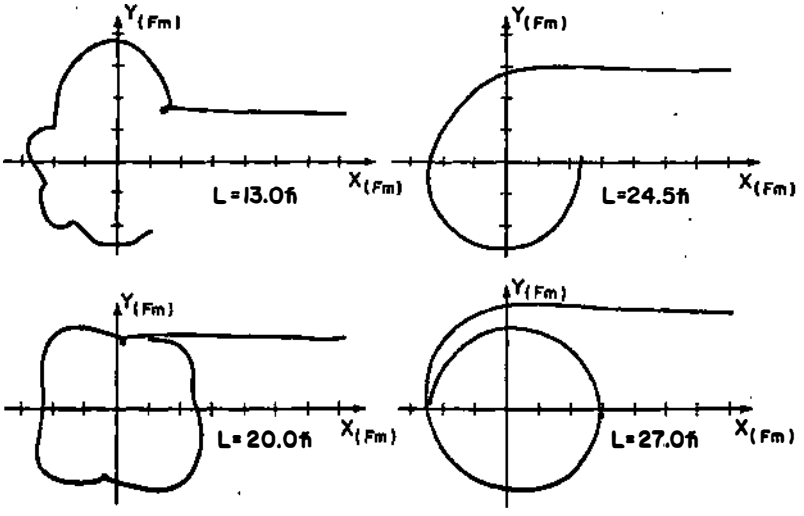

Fig. 7: As Fig. 6 for some of the trajectories that fused.

XBL777-1521

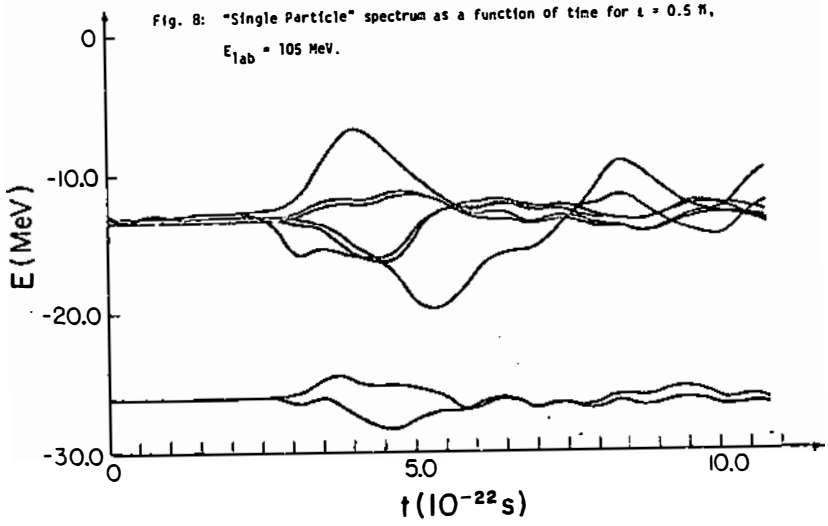

Fig. 8: "Single Particle" spectrum as a function of time for $\ell = 0.5\ \hbar$, $E_{lab} = 105$ MeV.

XBL777-1520

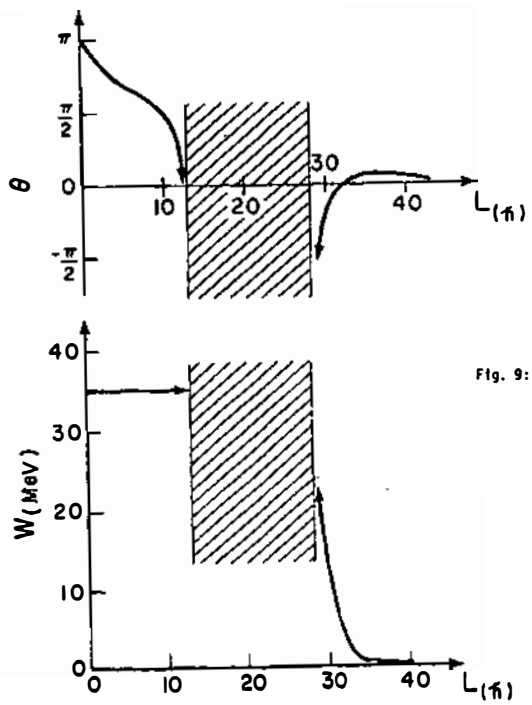

Fig. 9: Deflection angle and energy loss for $O^{16} + O^{16}$ at $E_{lab} = 105$ MeV vs initial angular momentum. Shaded region corresponds to fusion.

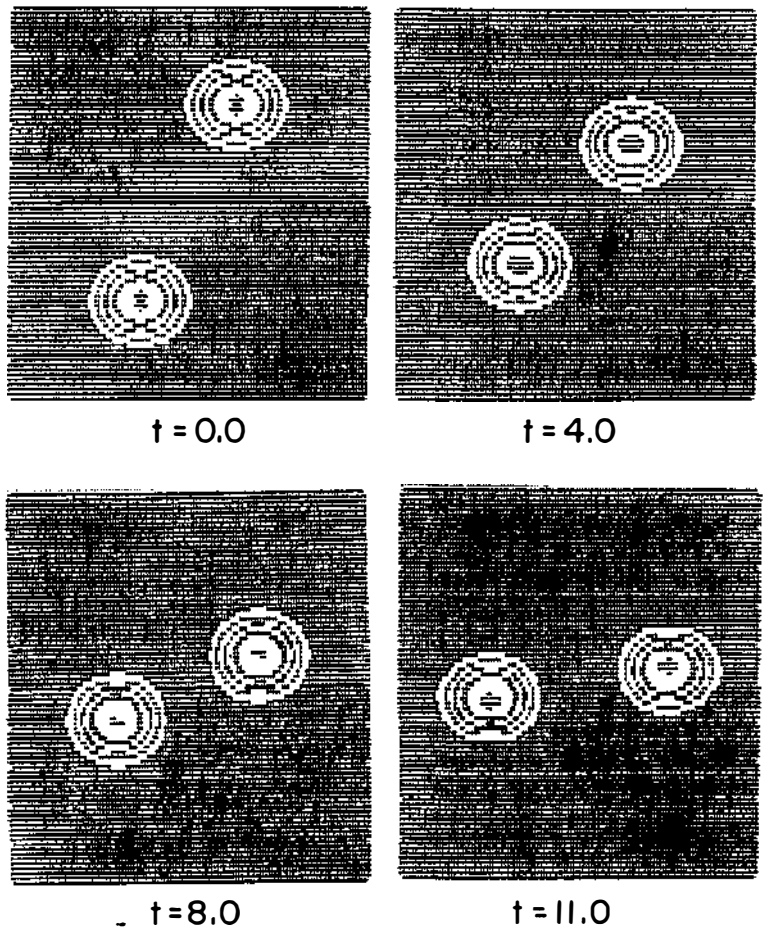

Fig.10: Density profile for $O^{16} + O^{16}$ at E_{lab} = 32 MeV, impact parameter 6 fm. Time is in units of 10^{-22} sec.

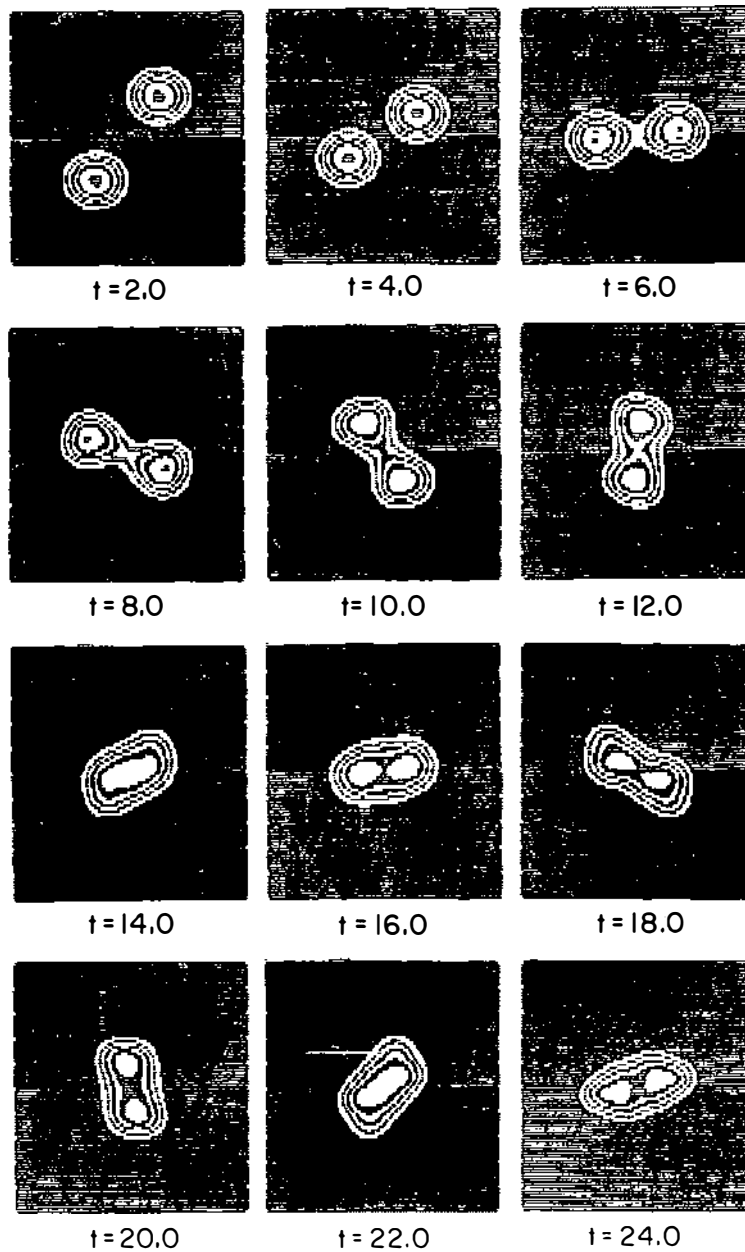

Fig. 11: Density profile for $O^{16} + O^{16}$ at E_{lab} = 64 MeV, impact parameter = 6 fm. Time is in units of 10^{-22} sec.

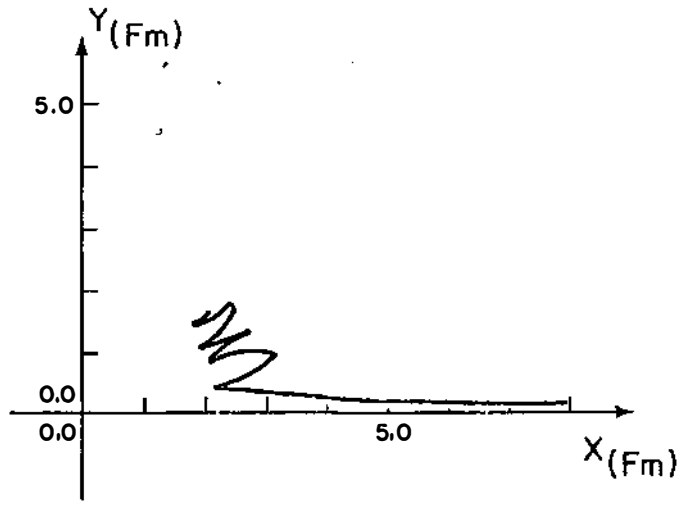

Fig. 12: Distance from the center of mass of the system of the center of mass of one fragment for the collision described in Fig. 11. Note how the vibration appears to slowly damp.

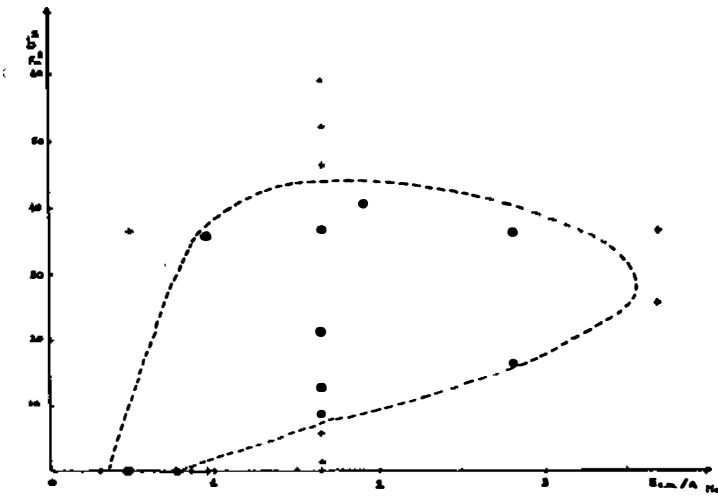

Fig. 14: Summary of the fusion region for $O^{16} + O^{16}$. Impact parameter, b squared is plotted against energy/nucleon in the center of mass. ● are points which have fused, + points which have scattered. The dotted line is estimate of fusion boundary.

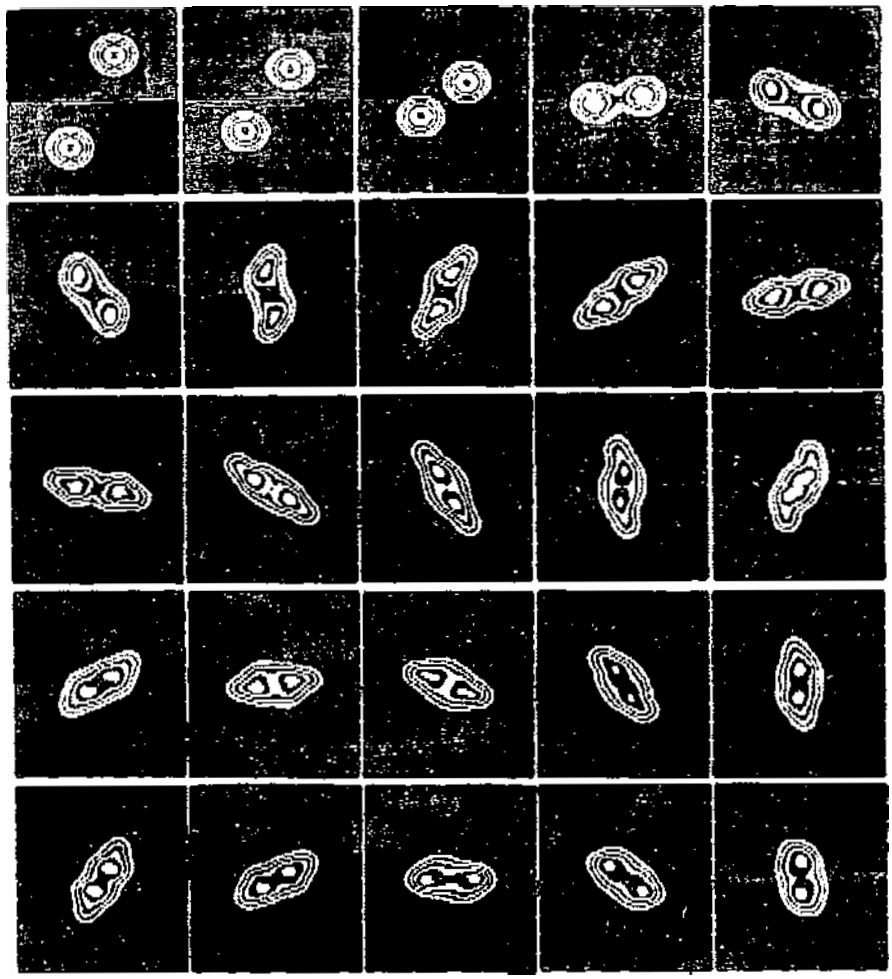

XBL 777-9651

Fig. 13: Density profile for $O^{16} + O^{16}$ at E_{lab} = 192 MeV, initial angular momentum 42 $\hbar$.

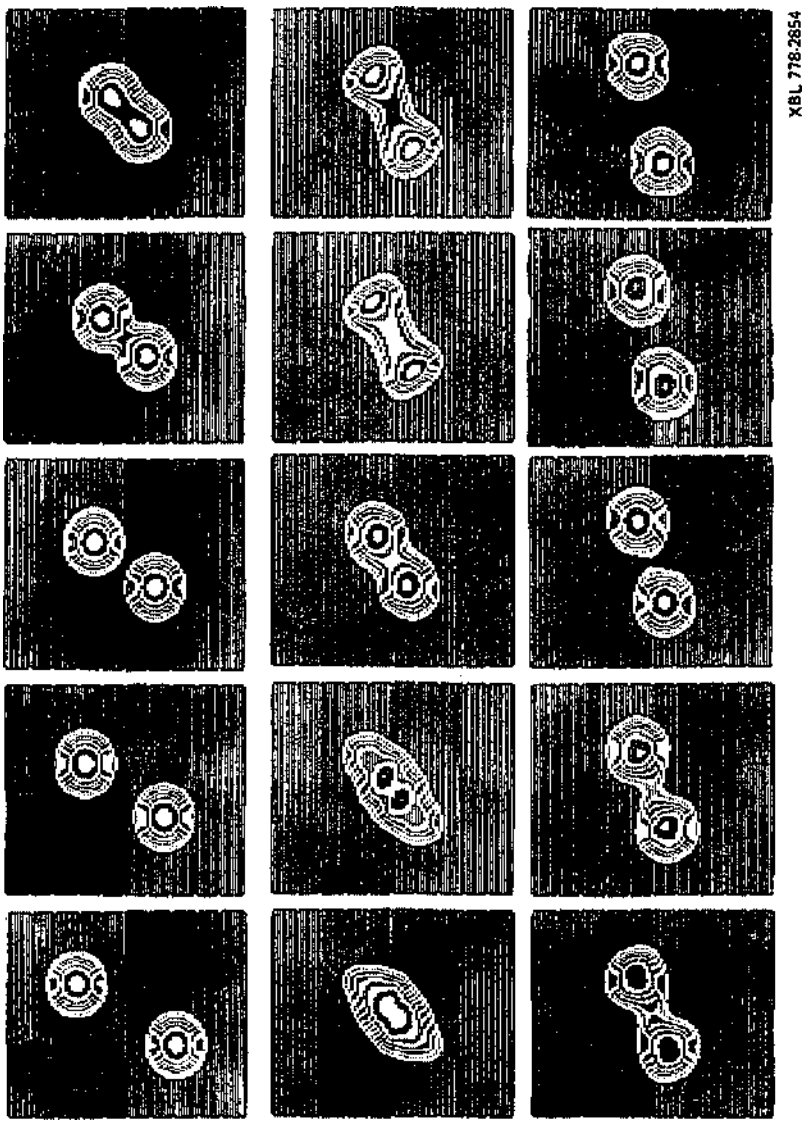

Fig. 15: Density profile for $Ca^{40} + Ca^{40}$ at E_{lab} = 278 MeV, incident angular momentum 20 $\hbar$.

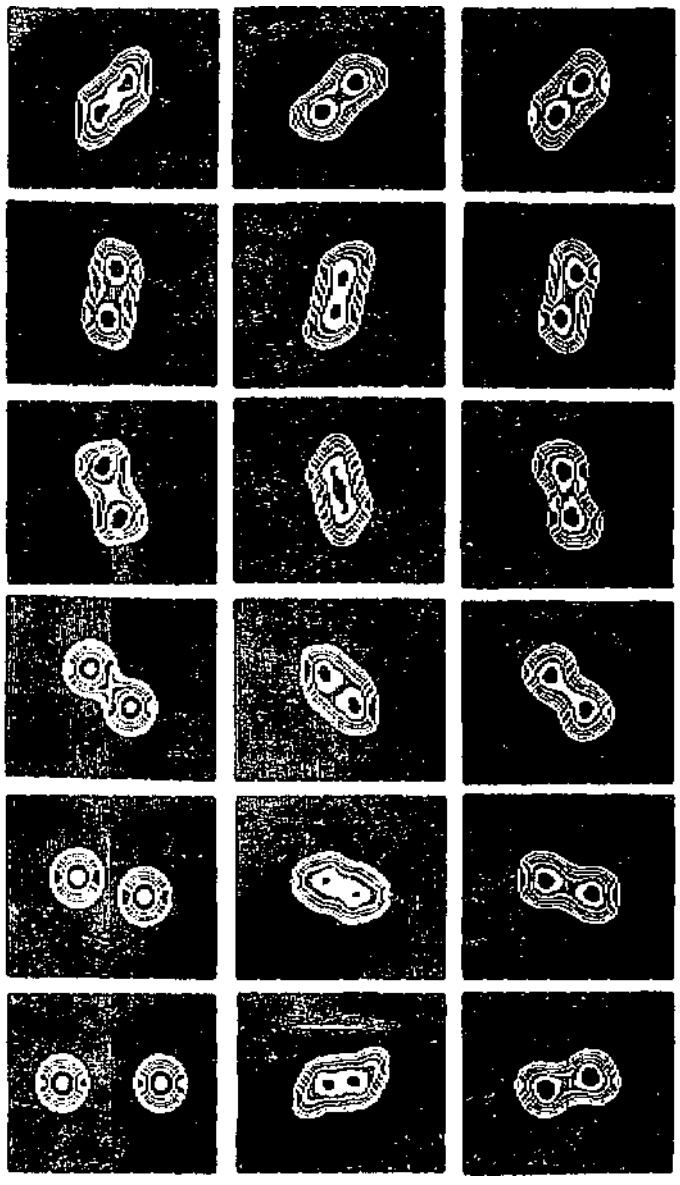

Fig. 16: As above, incident angular momentum 70 ħ.

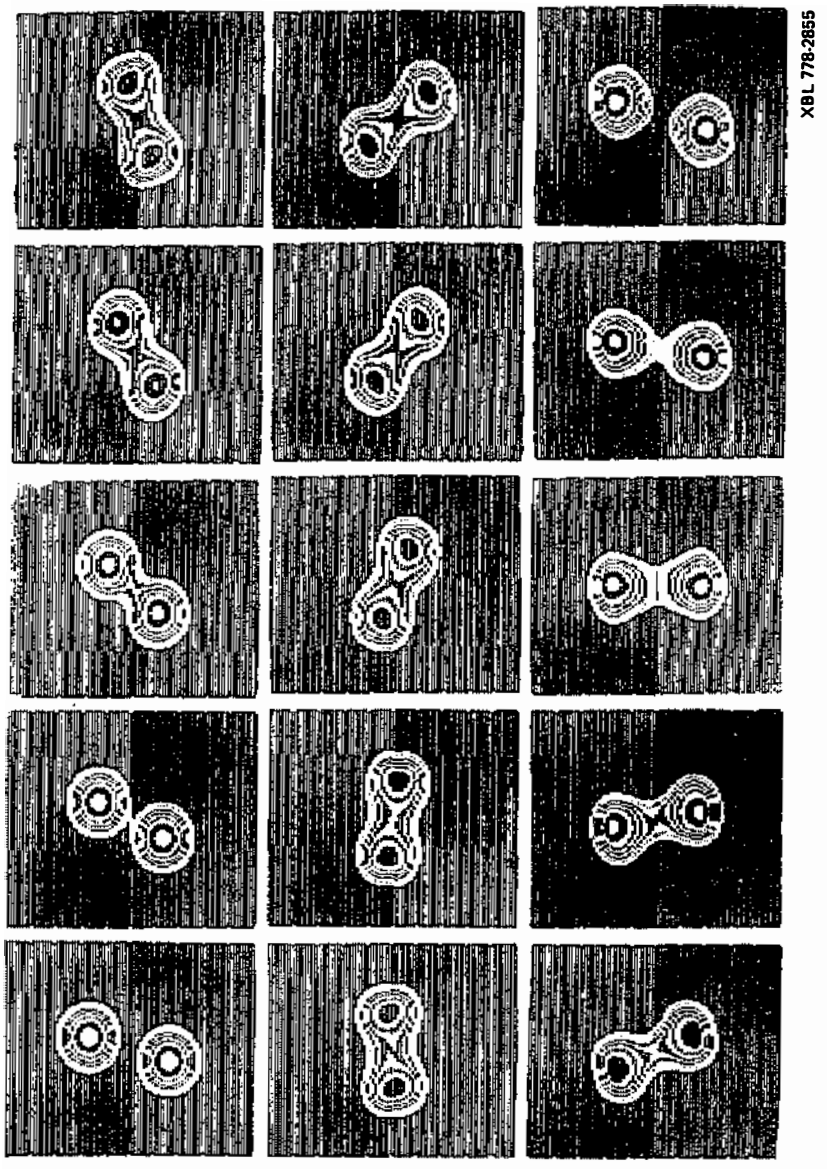

Fig. 17: As above, incident angular momentum 75 ħ.

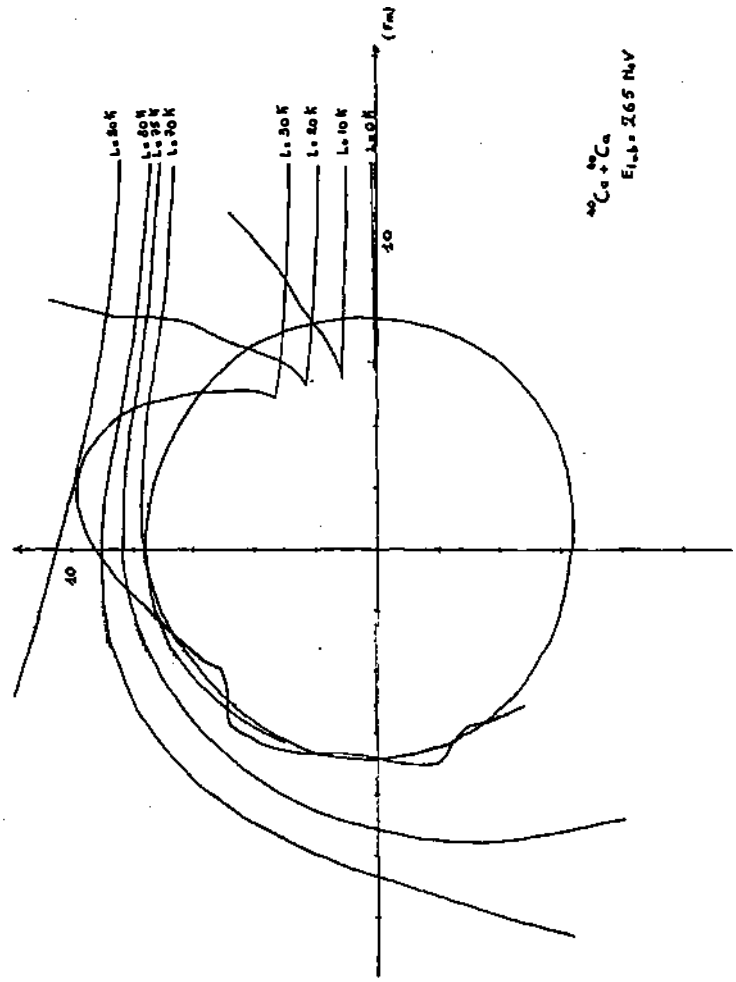

Fig. 18: Vector of the distance between the centers of mass of the two fragments for $Ca^{40} + Ca^{40}$, E_{lab} = 278 MeV for various impact parameters. Note that the structure for ℓ = 30 ħ is very similar to the corresponding orbits for $O^{16} + O^{16}$ at the onset of fusion. ℓ = 70 ħ corresponds to a scattering angle less than -3r.

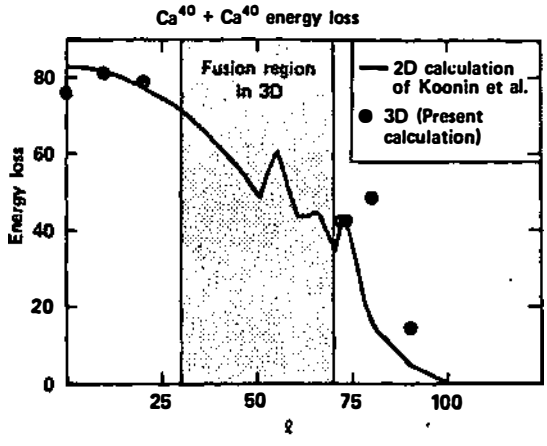

Fig. 19: The solid cruve is the energy loss from the 2D calculation of Ref. 2. The are the results of our 3D calculation for the same dynamic system. The major difference is the region of fusion found in 3D but not in 2D.

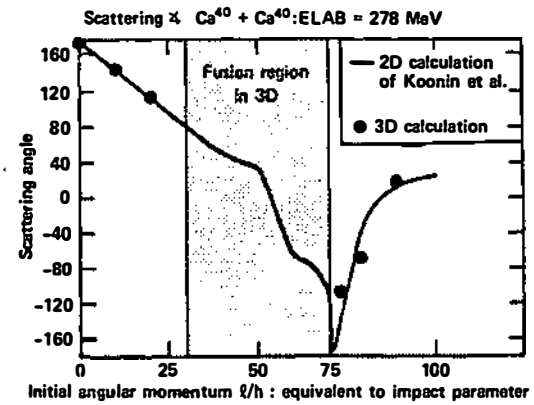

Fig. 20: The solid curve is the scattering angle from the 2D calculation of Ref. 2. The ● are the results of our 3D calculation. As in Fig. 19, the major discrepancy is in the region of fusion found in 3D but not in 2D.

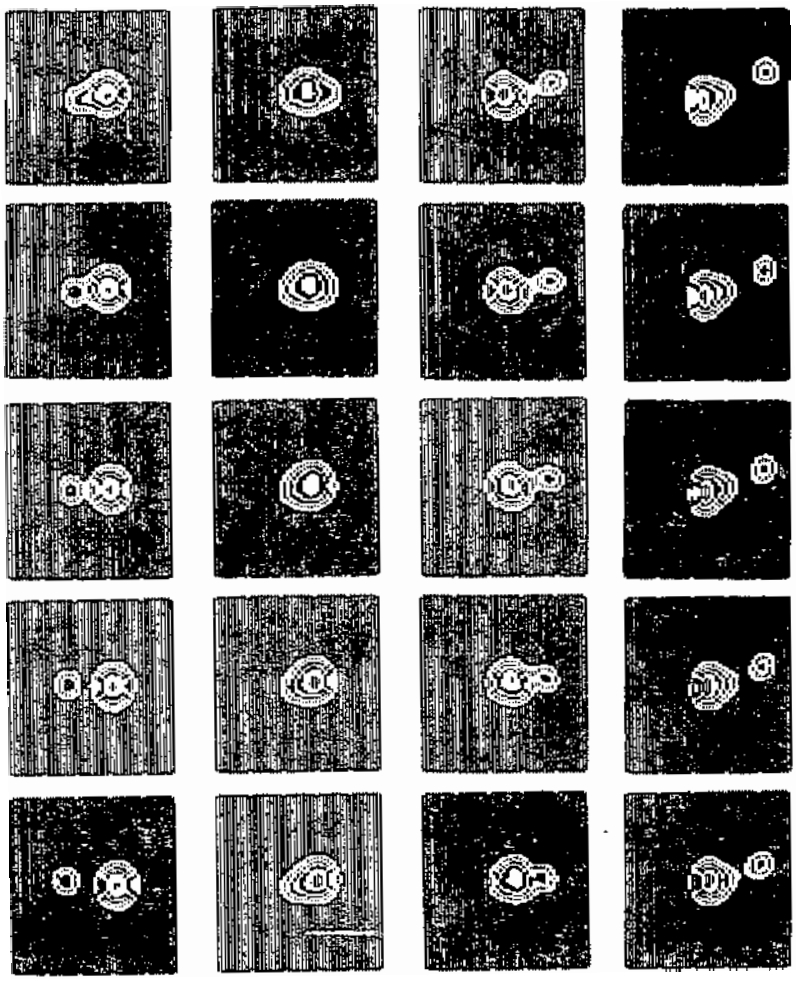

XBL 778-2949

Fig. 21: $He^4 + O^{16}$ at $\ell = 5\hbar$, $E_{lab} = 50$ MeV.

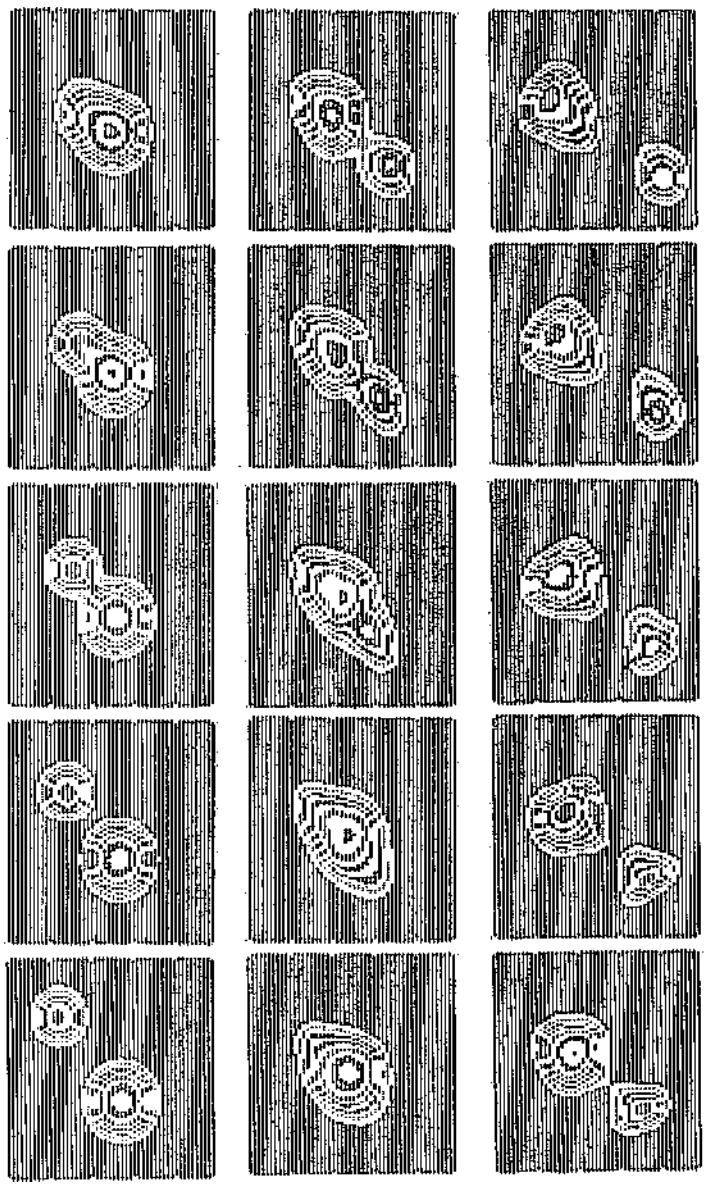

XBL 778-2952

Fig. 22: $O^{16} + Ca^{40}$ at $\ell = 20\,\hbar$, $E_{lab} = 315$ MeV.

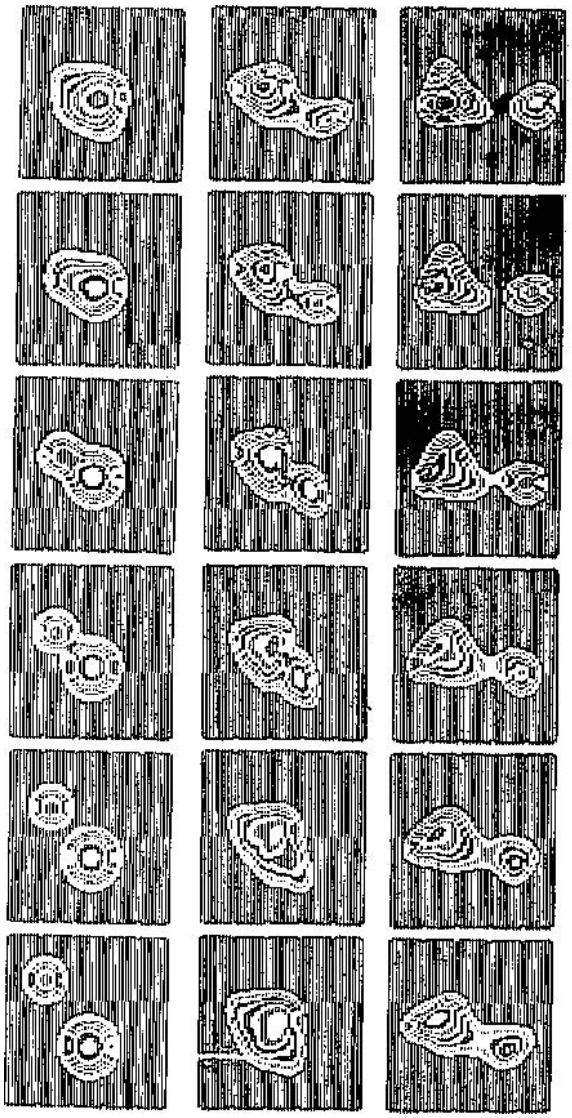

XBL 778-2950

Fig. 23: $O^{16} + Ca^{40}$ at $\ell = 40\ \hbar$, $E_{lab} = 315$ MeV.

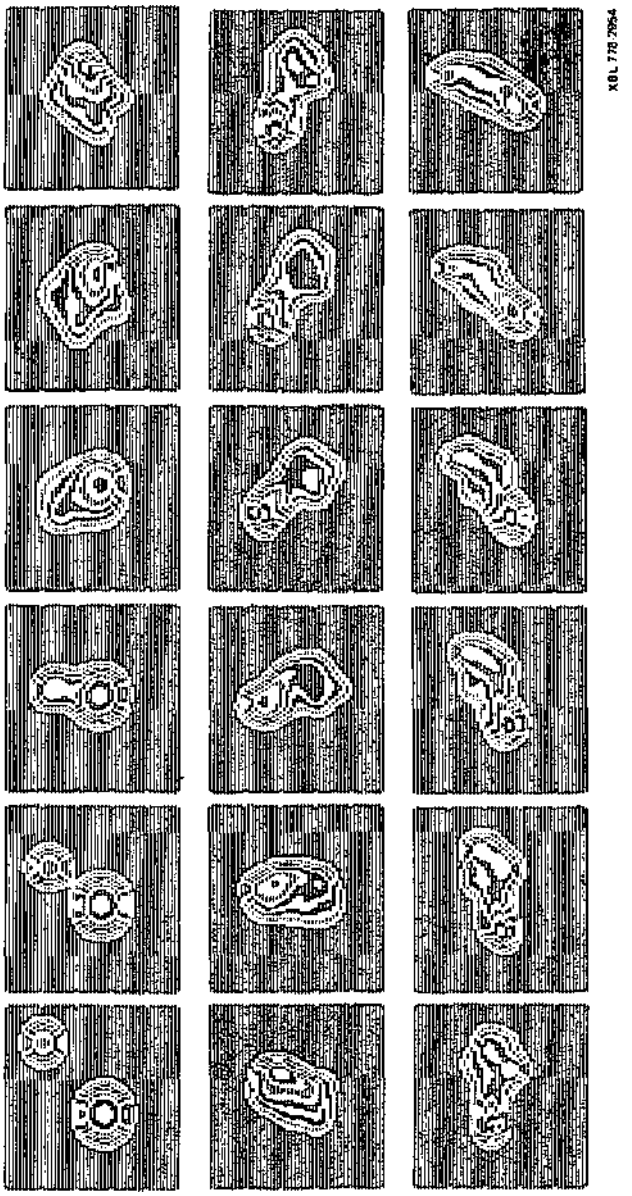

Fig. 24: $O^{16} + Ca^{40}$ at $\ell = 60\hbar$, $E_{lab} = 315$ MeV.

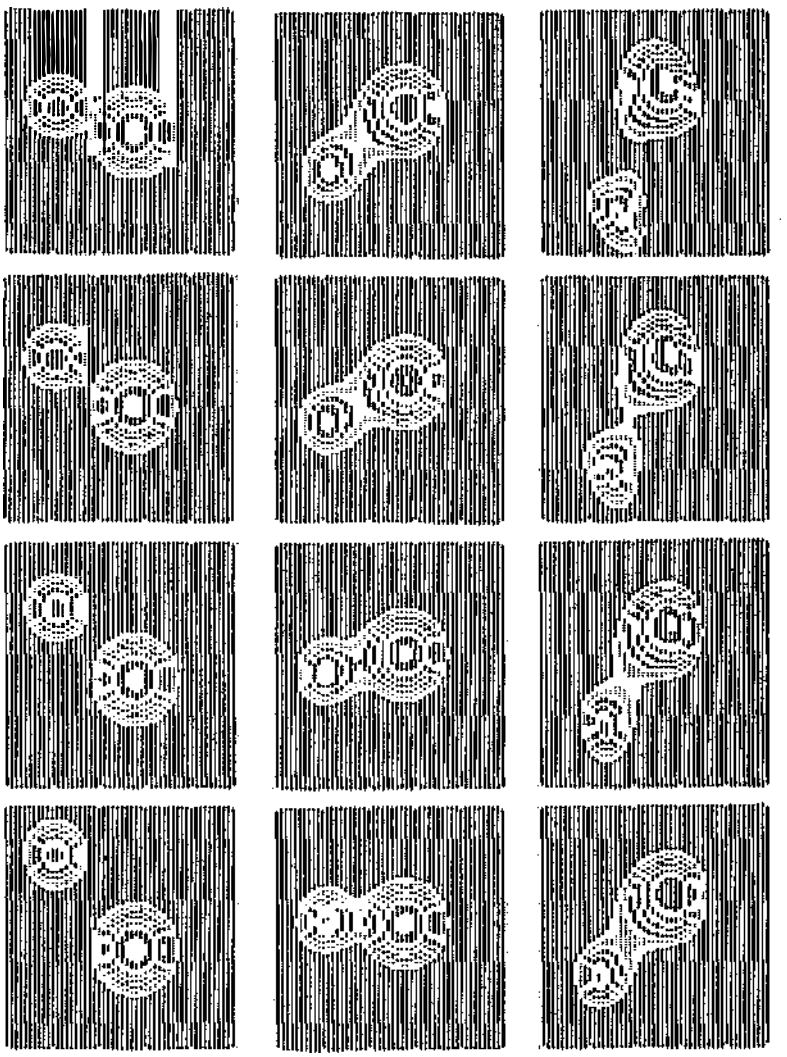

XBL 778-2953

Fig. 25: $O^{16} + Ca^{40}$ at $\ell = 80\ \hbar$, $E_{lab} = 315$ MeV.

DISCUSSION

J.J. Griffin: You said that your average potential protrudes outside the density by about 1 Fermi. Does that mean that you are performing your Hartree-Fock calculations with genuine finite range forces?

M.S. Weiss: Yes, but of a special spatial form, a Yukawa, adjusted so as to have no exchange term.

K. Goeke: I would like to mention that also in static HF and even in static HFB calculations in very large configuration spaces Yukawa-like interactions are being used. Many of those calculations are performed by D. Gogny in Paris. The use of finite range interactions for TDHF is particularly important since just the finite range terms cause the difference in mass between a more realistic ATDHF and the simple Inglis-model.

D.R. Thompson: Neither you nor dr. Maruhn in the previous talk mentioned reaction effects. I wonder why you don't see, for example, ^{28}Si and an α - particle come out when you let your ^{16}O nuclei collide. Is this because you have not included enough freedom in your description of ^{16}O?

M.S. Weiss: The final separated fragments individually are not eigenstates of the number operator. Each represents a distribution over final masses and would include ^{28}Si, say, in accordance with the width of the mass distribution.

J. Németh: What happens to the incoming kinetic energy of the projectiles when they come apart after a short time fusion?

M.S. Weiss: If they nearly fuse then they separate with a very large loss of the initial kinetic energy into internal motion of the fragments.

G. Grégoire: In the $^{40}Ca + ^{40}Ca$ case, could you tell me what are the central densities when the two nuclei merge together?

M.S. Weiss: We did not see any appreciable increase in density over that of the initial separated Hartree-Fock solutions central density. The nuclei expand during the collision rather than increase in density. We have not yet examined higher energies.

H. Stöcker: Can you calculate also higher energy head-on collisions (E_{LAB}/nucleon $\gtrsim$ 50 MeV) and what are the densities and excitation energies in these cases compared to the shock-wave calculations, where we see a doubling of the density at $E_{LAB}/n \approx 70$ MeV with exitation energies of about 18 MeV?

M.S. Weiss: Such an energy (E_{cm}/nucleon $\gtrsim$ 25 MeV) is at the upper limit of TDHF. I would be very suspicious of results at thatenergy. At lower energies (E_{cm}/nucleon $\approx$ 4 MeV) we do not see any appreciable density increase.

K. Dietrich: One of the most important questions concerning the applicability of TDHF is the importance of the term g_2 of Maruhn's presentation, i.e. the two-body collision term. In principle, one could - for testing the validity of neglecting this term - study within TDHF, the simple system of a (low energy) neutron impinging on a nucleus. Then the TDHF equation would predict the emission of a nucleon after a certain time which could be compared with the experimentally known lifetime of the system. My question is: would such a calculation be feasible?

M.S. Weiss: Yes, but perhaps not meaningful.

K. Goeke: Prof. Greiner rose the question if it is worthwhile to spend time in TDHF. To my feeling one can only answer this question if we really know what TDHF gives us besides nice pictures of moving density distributions. This means: today there is missing a theory which precisely tells which observables can be reliably calculated by TDHF, or, can we construct in an easy way effective operators for TDHF. Hopefully there are some.

M.S. Weiss: The properties of TDHF will only be ascertained by doing TDHF.